Selective Actuation of Arrays of Carbon Nanotubes Using Magnetic Resonance

Alexander Volodin,[†,*] Claudia A. Santini,[†,‡,§] Stefan De Gendt,[‡,⊥] Philippe M. Vereecken,[‡,∥] and Chris Van Haesendonck[†]

[†]Laboratory of Solid-State Physics and Magnetism, KU Leuven, Celestijnenlaan 200 D, BE-3001 Leuven, Belgium, [‡]IMEC, Kapeldreef 75, BE-3001 Leuven, Belgium, [§]IBM Zurich, Säumerstrasse 4, CH-8803 Rüschlikon, Switzerland, [⊥]Department of Chemistry, KU Leuven, Celestijnenlaan 200 F, BE-3001 Leuven, Belgium, and [∥]Centre for Surface Chemistry and Catalysis, KU Leuven, Kasteelpark Arenberg 23, BE-3001 Leuven, Belgium

ABSTRACT We introduce the use of ferromagnetic resonance (FMR) to actuate mechanical resonances in as grown arrays of carbon nanotubes (CNTs) loaded with Ni particles (Ni-CNTs). This contactless method is closely related to the magnetic resonance force microscopy technique and provides spatial selectivity of actuation along the array. The Ni-CNT arrays are grown by chemical vapor deposition and are composed of homogeneous CNTs with uniform length (~600 nm) and almost equal diameter (~20 nm), which are loaded with Ni catalyst particles at their tips due to the tip growth mode. The vibrations of the Ni-CNTs are actuated by relying on the driving force that appears due to the FMR excited at about 2 GHz in the Ni particles (diameter ~100 nm). The Ni-CNT oscillations (frequency ~40 MHz) are detected mechanically by atomic force microscopy. The acquired oscillation images of the Ni-CNT uniform array reveal clear maxima in the spatial distribution of the oscillation amplitudes. We attribute these maxima to the "sensitive slices", *i.e.*, the spatial regions of the Ni-CNT array where the FMR condition is met. Similar to magnetic resonance imaging, the sensitive slice is determined by the magnetic field gradient and moves along the Ni-CNT array as the applied magnetic field is ramped. Our excitation method does not require the presence of any additional microfabricated electrodes or coils near the CNTs and is particularly advantageous in cases where the traditional electrical actuation methods are not effective or cannot be implemented. The remote actuation can be effectively implemented also for arrays of other magnetic nanomechanical resonators.

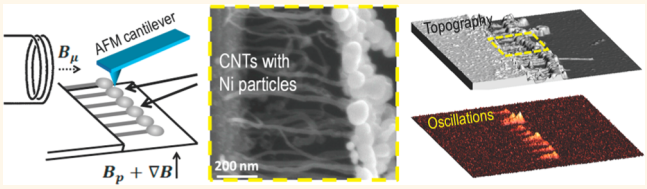

KEYWORDS: carbon nanotubes · carbon nanotube arrays · mechanical resonance · ferromagnetic resonance · magnetic resonance force microscopy · NEMS

Free-standing carbon nanotubes (CNTs) provide unique capabilities as high-frequency mechanical resonators for a number of sensing applications.[1,2] Although substantial progress has been made in using high-frequency CNT resonators,[3−6] their actuation remains challenging. The actuation of CNT resonators becomes even more challenging when using CNT arrays for sensing applications,[7] where the large number of sensing elements provides an increase of the sensitivity,[8] as well as for imaging and data processing technologies.[9] Different actuation methods are available for CNT resonators, including electrical capacitive *ac* actuation,[10,11] the recently proposed *dc* field emission actuation,[12,13] and acoustic actuation.[14] In the case of the most frequently used *ac* electrical actuation, an electrical signal has to be applied to electrodes placed close to the CNTs. A similar nearby counter electrode is necessary for the *dc* field emission actuation method.[13] The fabrication of the electrodes, which have to be able to carry high-frequency signals close to single CNTs or arrays of CNTs, is far from trivial. On the other hand, when the CNTs are grown after the electrode fabrication, the high temperatures necessary for CNT chemical vapor deposition (CVD) based growth may alter the mechanical integrity and the electrical performance of the electrodes. Moreover, the poor control of the CNT growth direction combined with the presence of a nearby electrode may cause a short circuit and result in defective devices.

Acoustic actuation as a contactless technique is potentially free from the aforementioned shortcomings and consequently may be applicable to arrays of CNT resonators. In this technique a vibrating substrate is used to induce CNT oscillations. Unfortunately, the frequency response of

* Address correspondence to Alexander.Volodine@fys.kuleuven.be.

Received for review January 25, 2013 and accepted June 3, 2013.

Published online June 03, 2013
10.1021/nn400412b

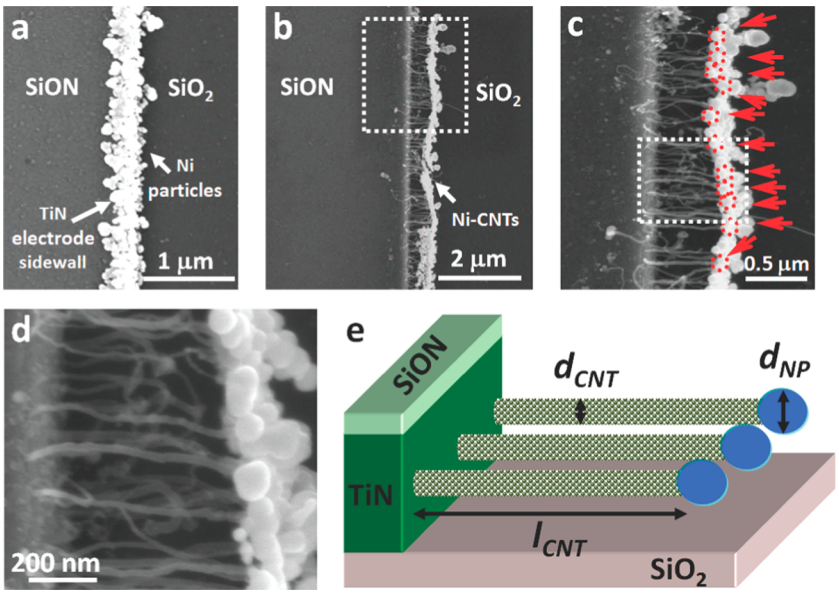

Figure 1. (a) SEM image of a Ni particle layer electrochemically deposited on the sidewall of a TiN electrode. (b) Low and (c and d) higher magnification views of the Ni-CNT array grown by CVD from the deposited Ni particles. (e) Schematic view of the Ni-CNT array.

the transducer-substrate system is very nonuniform and becomes rapidly attenuated at higher frequencies. A high-voltage driving signal is therefore required, which can interfere with the detection signal. Another contactless technique is based on optical[15] and magnetic actuation.[16,17] The primary excitation mechanism of optical actuation is of thermal origin.[15] Due to the high thermal conductivity of CNTs, it is difficult to achieve effective optical excitation which is based on nonuniform thermal expansion of the device material. Magnetic actuation of freely suspended CNTs can be achieved by using an external *ac* magnetic field that interacts with submicrometer magnetic particles that need to be attached to the CNTs. In this case, the CNT resonators can be actuated using two different approaches. In a first approach, a submicrometer magnetic particle interacts with a strong magnetic field gradient. A microscopic coil arranged in close proximity of the CNTs is needed to create such a gradient. The microfabrication of the coils is even more challenging than the microfabrication of electrodes suited for high-frequency electrical actuation. A second approach relies on a "gradient free" arrangement in which the CNT resonator is driven in "torque mode",[18] *i.e.*, torque induced deflection of the resonator with a magnetized particle in a homogeneous *ac* magnetic field. This approach may not be applicable for submicrometer particles, which are attached to the CNTs, because such small particles typically are superparamagnetic with their magnetic moment aligned along the vector field resulting from the applied *dc* and *ac* fields.

In this paper, we introduce a novel contactless actuation method for CNT arrays loaded with Ni particles (Ni-CNTs), which does not require any additional nearby electrodes or coils. The proposed method relies on the mechanical actuation of the Ni-CNTs that are under ferromagnetic resonance (FMR) in an external inhomogeneous magnetic field. This method is closely related to the magnetic resonance force microscopy (MRFM) technique.[19,20] The MRFM technique is based on the force interaction between a time dependent resonating magnetic moment of a sample, which is mounted on a compliant micromechanical resonator, and an inhomogeneous external magnetic field.[19] We use the dynamic mode atomic force microscopy (AFM) technique for detecting the high-frequency mechanical resonances of the Ni-CNT arrays.[21,22] Our method is successfully applied to actuate an as grown uniform high-density array of CNT mechanical resonators. Furthermore, our method offers spatial selectivity for actuating different parts of the array.

RESULTS AND DISCUSSION

The Ni-CNT arrays are grown by CVD from Ni catalyst particles obtained by electrochemical deposition (ECD) on the sidewalls of titanium nitride (TiN) electrodes.[24−27] CNTs are grown by CVD underneath the Ni particles that are lifted off from the TiN electrode sidewalls due to the tip growth mode (see Figure 1b−d), thus remaining horizontally freestanding and loaded with Ni particles at their tips. Scanning electron microscopy (SEM) images of an as-grown Ni-CNT array are presented in Figures 1a−d. The homogeneous CNT growth rate produces CNTs with comparable lengths l_{CNT} (around 600 nm) and almost equal diameters d_{CNT} (about 20 nm), as schematically indicated in Figure 1e. The length of the Ni-CNT arrays is determined by the length of the electrodes, as the Ni-CNTs uniformly grow from

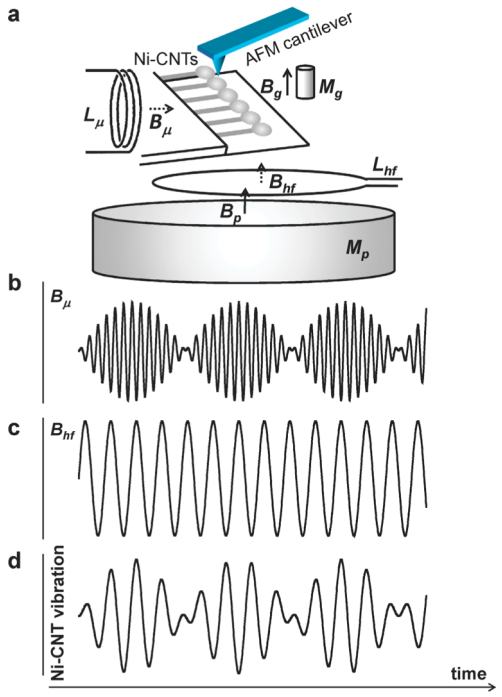

Figure 2. (a) Schematic view of the setup for the actuation and the detection of the mechanical resonances of a Ni-CNT array. (b–d) Time dependence of the different signals that are applied in the setup presented in (a); (b) amplitude modulated microwave magnetic field B_μ generated by the coil L_μ; (c) magnetic field modulation produced by the coil L_{hf}; (d) the resulting Ni-CNT oscillation.

the electrode sidewalls which are as long as 100 μm. The corresponding linear density of the Ni-CNT arrays is determined to be 25 $\pm$ 5 Ni-CNTs/μm.

In Figure 2a, we present a scheme of the setup for actuation and detection of the mechanical resonances of the Ni-CNT arrays. A polarizing magnetic field B_p produced by a magnet M_p is applied to the sample with the Ni-CNT array in order to align the Ni particle spins. A microwave magnetic field B_μ generated by a nearby coil L_μ is oriented perpendicularly to B_p. The frequency f_μ of B_μ is resonant with spins in the Ni particles in which the polarizing field induced spin energy level splitting equals the energy of the microwave radiation. The oscillations of the Ni-CNTs are driven by modulating the polarizing magnetic field with amplitude B_{hf} and frequency f_{hf}. The frequency of the amplitude modulation of B_μ is set to enable the AFM detection of the Ni-CNT oscillations, as will be explained below. A small permanent magnet M_g arranged in close vicinity of the Ni-CNT array is used to produce a spatially inhomogeneous magnetic field which plays two important roles: (i) it couples the Ni-CNT mechanical resonator to the magnetic moments in the Ni particles,[28] and (ii) it defines the spatial regions of the Ni-CNT array where the FMR condition is met. Through the gradient-dipole force between the Ni particle spins and the magnet M_g, the cyclic spin inversion drives the Ni-CNTs into modulated oscillations[29] as plotted schematically in Figure 2d. When the driving modulation frequency f_{hf} approaches the mechanical resonance frequency (f_{MR}) of one of the Ni-CNTs, the amplitude A of its oscillations becomes large with an amplification factor proportional to the quality factor Q of the Ni-CNT resonator.

The Ni-CNT oscillations are mechanically detected by AFM operating in dynamic mode.[21] The AFM cantilever is unable to follow the fast (MHz) oscillations of the Ni-CNTs. Nevertheless, it is able to detect the envelope of the amplitude modulated Ni-CNT oscillations due to the nonlinear relation between the force exerted on the AFM cantilever and the sample-tip distance. The AFM detection sensitivity is enhanced by matching the amplitude modulation frequency of B_μ to the fundamental resonance frequency of the AFM cantilever. Similar to Reference[23] the second eigenmode of the cantilever (f_{cant2} = 380 kHz) is used to provide standard AFM operation and topography imaging, whereas the Ni-CNT oscillation imaging is realized at the cantilever fundamental frequency (f_{cant1} = 60 kHz). Finally, the dynamic AFM mode set point and oscillation amplitude are adjusted to minimize the influence of the parasitic forces acting between the Ni-CNT and the AFM tip.[21] To increase the detection sensitivity, the measurements are performed in He gas atmosphere (which provides a 2 times enhancement of the Q-factors of the Ni-CNT resonators).

In Figure 3, we present an AFM topography image of a Ni-CNT array (Figure 3a) and the corresponding oscillation image (Figure 3b). Note that the imaged sample region is the one corresponding to the SEM image in Figure 1c. The topographic AFM image reveals that the CNTs form a quite uniform array parallel to the substrate with Ni particles clearly visible at their tips. The oscillation image has a color contrast that reflects the oscillation amplitude of the Ni-CNTs. This contrast is maximized by tuning f_{hf} in order to reach the mechanical resonance condition for the majority of the Ni-CNTs in the array. Note that the most pronounced contrast appears at the free tips of the Ni-CNTs, while a few Ni-CNTs are kept together by the Ni deposit at their tips. The oscillation amplitude of the latter Ni-CNTs is considerably smaller and is not visible in the oscillation image in Figure 3b.

In Figure 3c, we present the mechanical resonance curve (oscillation amplitude A *versus* f_{hf}) obtained for the Ni-CNT indicated by the arrow in Figure 3b. The mechanical resonance occurs at a frequency f_{MR} of 45 MHz. To determine the quality factor Q, we fit the measured resonance curve to a Lorentzian curve. For the Ni-CNT indicated by the arrow in Figure 3b, Q is around 17.

In Figure 3d, we plot the dependence of the oscillation amplitude A on the polarizing magnetic field B_p. The dashed line corresponds to a fit based on a Lorentzian shape of the FMR signal, which allows to

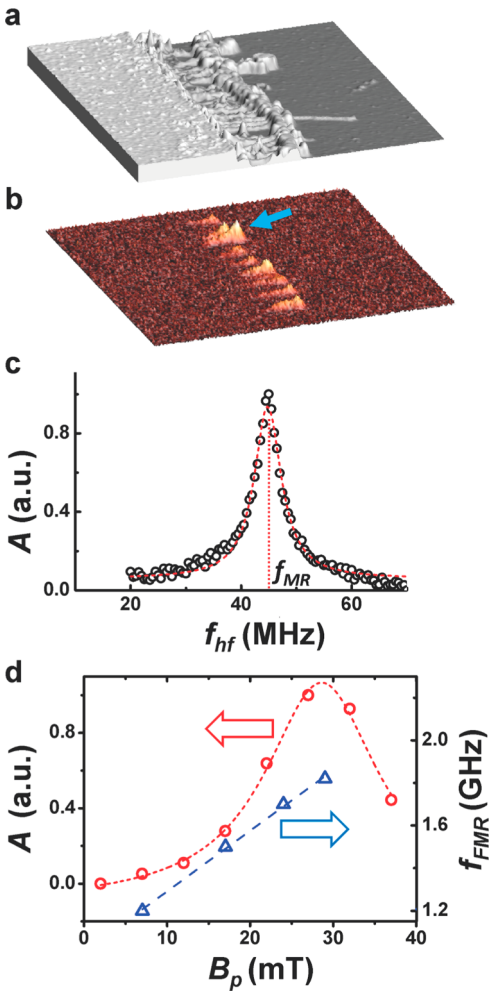

Figure 3. (a) A 3.75 × 3.75 μm^2 AFM topography image and (b) corresponding oscillation image for the Ni-CNT array presented in Figure 1c. (c) Mechanical resonance curve obtained for the Ni-CNT indicated by the arrow in (b). (d) Oscillation amplitude A and FMR frequency f_{FMR} as a function of the polarizing magnetic field B_p.

determine the ferromagnetic resonance field corresponding to the ferromagnetic resonance frequency f_{FMR}. The FMR line width $\Delta B \sim 10$ mT, which we infer from this fit, corresponds to the typical value obtained for Ni nanoparticles with a high degree of structural disorder.[30] Note that the widening of the FMR resonance resulting from the magnetic field gradient can be neglected due to the small size of the Ni particles. Similar measurements were performed at different microwave frequencies f_{FMR} and the obtained f_{FMR} on B_p dependence is plotted in Figure 3d. Our results demonstrate that the FMR frequency f_{FMR} depends linearly on B_p. The $f_{FMR}(B_p)$ plot also reveals the presence of an offset field. This result is consistent with the field dependence of f_{FMR} for a spherical ferromagnetic particle:[31]

$$f_{FMR} = \gamma(B_P + B_{off}) \qquad (1)$$

where γ is the effective gyromagnetic ratio ($\gamma/2\pi = 28$ MHz/mT) and $B_{off} = 33$ mT is an offset in the polarizing magnetic field that can be attributed to the vertical

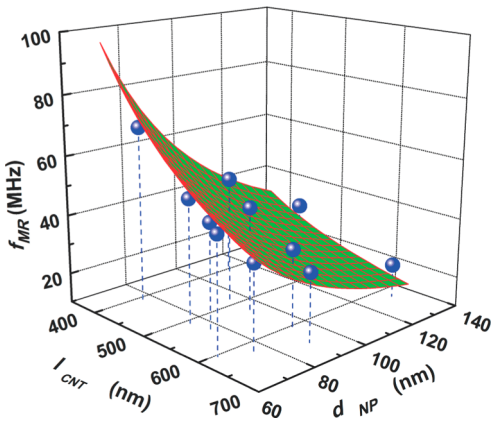

Figure 4. 3D plot of the mechanical resonance frequencies f_{MR} of the Ni-CNTs indicated by the red arrows in Figure 1c as a function of d_{NP} and l_{CNT}, and the related fit (green surface) of the data, which is based on eq 2 assuming that m_{CNT} is much smaller than m_{NP}.

component of the magnetic field B_g that is generated by M_g (see Figure 2a). This confirms the validity of our experimental procedure as a reliable actuation method of the Ni-CNT arrays by means of FMR induced in the Ni particles.

If we model a Ni-CNT as a cylindrical elastic beam with an additional mass concentrated at its tip (the Ni particle), the fundamental mechanical resonance frequency f_{MR} of the Ni-CNT resonator can be expressed as[32]

$$f_{MR} = \sqrt{\frac{3\pi E d_{CNT}^4}{64 l_{CNT}^3 (m_{NP} + 0.24 m_{CNT})}}$$

$$\approx \frac{d_{CNT}^2}{8}\sqrt{\frac{3\pi E}{l_{CNT}^3 m_{NP}}} = \frac{d_{CNT}^2}{8}\sqrt{\frac{18E}{\rho_{Ni} d_{NP}^3 l_{CNT}^3}} \qquad (2)$$

where E is the Young modulus of the CNT, d_{CNT}, l_{CNT}, and m_{CNT} are the diameter, the length, and the mass of the CNTs, respectively (see Figure 1e), d_{NP} and m_{NP} are the diameter and the mass of the Ni particles, respectively, and ρ_{Ni} is the specific mass density of Ni.

In Figure 4, we present a 3D plot of the mechanical resonance frequencies f_{MR} of the Ni-CNTs as a function of d_{NP} and l_{CNT}. The resonance frequencies are measured for the set of 11 Ni-CNTs indicated by the red arrows in Figure 1c. The measured data are fitted using eq 2 in the limit $m_{CNT} \ll m_{NP}$, confirming the dependence of the frequency f_{MR} on the length of the CNTs and the mass of the Ni particles. The best fit of the data upon variation of d_{NP} and l_{CNT} corresponds to a Young modulus of the CNTs of about 90 GPa, which is in the range of the previously measured Young modulus of CVD grown CNTs.[33] We finally note that the different amplitude of the oscillations of the Ni-CNTs imaged in Figure 3b has to be attributed to the different geometrical parameters of the oscillators, primarily the CNT lengths and the Ni particle masses.

An important question arises concerning the possible sensing applications of our Ni-CNT arrays. Two key

parameters are responsible for the sensitivity of resonant mass sensors: i) the effective mass of the resonator and ii) the stability of its resonance frequency.[34] Minimizing the effective mass of the resonator and maximizing the stability of its resonance frequency are especially desirable for mass sensing applications, as the smallest detectable mass is given by $\Delta m \approx 2 m_{RES} \times (\Delta f/f_{MR})$,[34] where m_{RES} is the effective mass of the resonator and $\Delta f/f_{MR}$ is the instability of its resonance frequency. In our configuration the mass of a Ni particle is $m_{NP} \sim 5$ fg, which is much larger than the mass of the CNT m_{CNT}. Consequently, the effective mass of the resonator is $m_{RES} \approx m_{NP}$. For a frequency instability which we estimate to be of about 3×10^{-3} (for the 3 ms averaging time employed), the smallest mass detectable by our resonators is $\Delta m \sim 30$ ag.

As mentioned, the sensitivity of our resonant mass sensor could be increased by decreasing m_{NP}. However, from a fabrication point of view, Ni particles with diameters as large as 100 nm are needed to guarantee the tip growth mode of all the CNTs in the array. This way, we ensure that the resulting Ni-CNT resonators have similar lengths and are all loaded with particles of similar size at their tips (see Methods). Another way to increase the sensitivity of our resonant mass sensor is to decrease its resonance frequency instability. The relatively high frequency instability is primarily determined by the low mechanical quality factor Q of our Ni-CNTs that is in the range of 10−20. The low Q may be attributed to the air drag. Indeed, our measurements performed in He gas atmosphere reveal a 2 times enhancement of the Q-factors of the Ni-CNT resonators. Similar low Q values were obtained for CNT resonators oscillating in air at atmospheric pressure, while the same CNT resonators measured in vacuum exhibited ~10 times higher Q-factors.[23] Therefore, we can assume that the Q-factors of our Ni-CNT resonators can be significantly enhanced by using a vacuum environment which would allow zeptogram-level mass detection.

Since our actuation technique is based on the force interaction between a time dependent resonating magnetic moment of a Ni particle and an inhomogeneous external magnetic field the force sensitivity of the Ni-CNT resonators is an important property for the efficiency of the actuation technique. The force sensitivity of the Ni-CNT resonators, or, strictly speaking, the minimum detectable force gradient is $\partial F/\partial z = 2k \times (\Delta f/f_{MR}) \sim 2.4 \times 10^{-3}$ N/m (k is the spring constant of the Ni-CNT). Note that the estimated sensitivity value is ~30 times smaller than the actuation force gradient which is evaluated from the experimental data.

We now turn to the spatial distribution of the oscillation amplitudes along the Ni-CNT array. In Figure 5a, we present a larger scale $10 \times 10\ \mu m^2$ AFM topography image of a Ni-CNT array. The corresponding oscillation

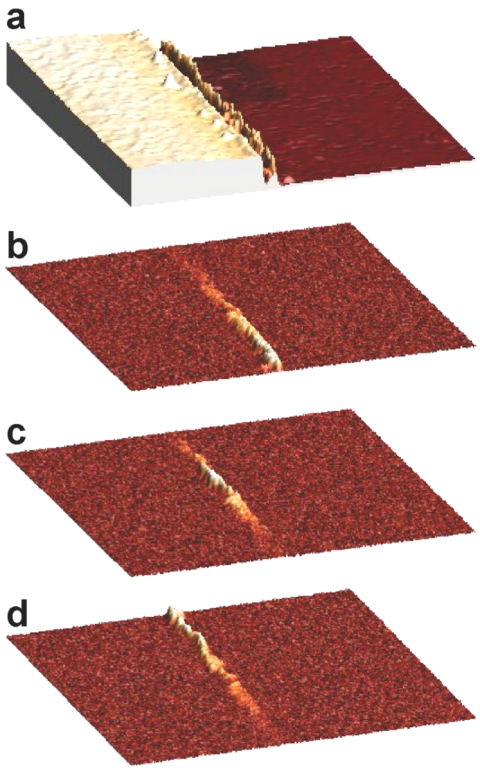

Figure 5. (a) A $10 \times 10\ \mu m^2$ AFM topography image and corresponding oscillation images of the Ni-CNT array acquired at different external magnetic fields B_p: (b) 25 mT, (c) 30 mT, and (d) 35 mT.

images acquired at different external magnetic fields B_p are presented in Figure 5b−d. The oscillation amplitudes of the individual Ni-CNTs cannot be resolved in these large scan area images. On the other hand, the oscillation images reveal clear maxima in the spatial distribution of the oscillation amplitudes. The maxima occur at different positions along the Ni-CNT array, depending on the applied magnetic fields B_p. We attribute this observation to the displacement of a "sensitive slice", *i.e.*, the spatial region of the Ni-CNT array where the ferromagnetic resonance condition is met.[19,20] Note that the observed spatial distribution in Figure 5b−d of the oscillation amplitudes cannot be attributed to the geometrical differences between different Ni-CNT resonators because the array is quite uniform and the driving frequency remains constant upon variation of B_p. Similar to MRFM the sensitive slice is defined by the magnetic field gradient and moves as the applied magnetic field is ramped.[19,20] We estimate that the magnetic field gradient due to the presence of the bar magnet M_g in the vicinity of the Ni-CNT array is approximately 400 T/m. For our 10 μm long Ni-CNT array, this corresponds to a field difference around 4 mT along the array. Because the FMR line width of the Ni particles, which is about 10 mT, is comparable to this difference, we are able to distinguish resonance signals arising from different spatial locations in the Ni-CNT array by means of the applied magnetic field gradient.

These results unambiguously demonstrate that our FMR-based actuation method provides spatially selective actuation of mechanical resonances in specific parts of the Ni-CNT arrays.

CONCLUSIONS

In conclusion, we demonstrated the effectiveness of a new contactless method to actuate CNT-based nanomechanical resonators. The method relies on the excitation of the ferromagnetic resonance of Ni particles present at the tips of freestanding CNTs. The Ni-CNTs form a large array of mechanical resonators with a high density and they may be used for sensing applications. Our actuation method offers spatially selective actuation of specific parts of the array of nanomechanical resonators. This can be particularly advantageous in cases where traditional actuation methods are not effective or cannot be implemented.

METHODS

Sample Fabrication. The Ni-CNT arrays are grown by CVD from Ni catalyst particles obtained by electrochemical deposition (ECD) on the sidewalls of TiN electrodes. The 200 nm thick TiN electrodes are deposited on SiO_2 (200 nm)/p^+ doped Si substrates. A 50 nm thick layer of silicon oxinitride (SiON) is deposited on top of the TiN electrodes in order to prevent CNT growth from the top of the electrodes. More details about the electrode structures, the growth method and the characterization of as-grown carbon nanotubes can be found in refs 24−27. An ECD potential of −3 V, which is applied for 1 s, enables the deposition of high-density (around 10^{12} cm^{-2}) and quite large (diameter around 100 nm) Ni catalyst particles (see Figure 1a). Next, CNTs are grown by CVD underneath the Ni particles that are lifted off from the TiN electrode sidewalls due to the tip growth mode (see Figures 1b−d). The growth of CNTs underneath the Ni particles suggests that the CNT nucleation is promoted under the Ni particle layer rather than on top of it. Carbon poisoning of the Ni top surface may be the reason for its inactivity as CNT growth catalyst. On the other hand, the Ni bottom surface is better protected from poisoning and is able to catalyze the CNT growth. To induce the tip growth of all the CNTs in the array, particles as large as 100 nm needed to be used. The tip growth mode provides a higher negative variation of free energy with respect to base growth mode only for particle size larger than a certain value, as it was recently found by Dijon *et al.*[35] In our experiments, particle diameters smaller than 80 nm rather catalyzed the base growth of carbon nanotubes and/or traces of metal catalyst remained along the carbon nanotube length.

Experimental Setup. A cylindrical permanent magnet M_p (2 cm in diameter) is placed close to the sample with the Ni-CNT array in order to produce a uniform polarizing magnetic field B_p that aligns the Ni particle spins. The value of B_p can be tuned between 3 and 50 mT by adjusting the distance between the magnet and the sample. A small coil L_μ (2 mm in diameter) is placed nearby in order to generate a microwave magnetic field B_μ (about 0.2 mT). B_μ is oriented perpendicularly to B_p and it is amplitude modulated, as illustrated in Figure 2b. The frequency of the amplitude modulation of B_μ (in the range of tens of kHz) is set to enable the AFM detection of the Ni-CNT oscillations, as will be explained below. On the other hand, the microwave frequency f_μ of B_μ can be tuned between 1 and 2 GHz (*L* band) to induce FMR in the Ni particles. A radio frequency coil L_{hf} is placed on top of the permanent magnet M_p. The coil is used to modulate the polarizing magnetic field with an amplitude B_{hf} and a frequency f_{hf} (in the MHz range), which sets the driving frequency for the Ni-CNTs. A small permanent magnet M_g (Sm−Co alloy cylinder with 0.5 mm diameter and 1 mm height) arranged in close vicinity (0.2−0.5 mm) of the Ni-CNTs is used to produce a spatially inhomogeneous magnetic field (B_g), which couples the magnetization of the Ni particles to the mechanical oscillations of the Ni-CNTs.[29]

For the AFM based measurements, we use a customized commercial scanning probe system (Autoprobe M5, Bruker) equipped with the Nanonis SPM controller (SPECS Zurich GmbH). Before imaging the oscillation amplitude, we first need to perform an optimization of the measured oscillation signal. First, a standard AFM topography image of the Ni-CNT array is acquired. Next, the AFM cantilever is placed above a Ni particle of interest. The microwave frequency f_μ is then set close to the expected value for FMR at given B_p and the driving frequency f_{hf} is swept between 10 and 80 MHz. As a result of recording the response of the cantilever, the mechanical resonance curve $A(f_{hf})$ of the chosen Ni-CNT is obtained. Further enhancement of the oscillation amplitude A is achieved by varying B_p and correspondingly tuning the FMR.

Conflict of Interest: The authors declare no competing financial interest.

Acknowledgment. This work was supported by the Research Foundation − Flanders (FWO, Belgium) as well as by the Belgian Interuniversity Attraction Poles (IAP) and the Flemish Concerted Action (GOA) research programs.

REFERENCES AND NOTES

1. Roukes, M. Nanoelectromechanical Systems Face the Future. *Phys. World* **2001**, *14*, 25–31.
2. Knobel, R. G.; Cleland, A. N. Nanometre-Scale Displacement Sensing Using a Single Electron Transistor. *Nature* **2003**, *424*, 291–293.
3. Poncharal, P.; Wang, Z. L.; Ugarte, D.; de Heer, W. A. Electrostatic Deflections and Electromechanical Resonances of Carbon Nanotubes. *Science* **1999**, *283*, 1513–1516.
4. Peng, H. B.; Chang, C. W.; Aloni, S.; Yuzvinsky, T. D.; Zettl, A. Ultrahigh Frequency Nanotube Resonators. *Phys. Rev. Lett.* **2006**, *97*, No. 087203.
5. Reulet, B.; Kasumov, A. Y.; Kociak, M.; Deblock, R.; Khodos, I. I.; Gorbatov, Y. B.; Volkov, V. T.; Journet, C.; Bouchiat, H. Acoustoelectric Effects in Carbon Nanotubes. *Phys. Rev. Lett.* **2000**, *85*, 2829–2832.
6. Nishio, M.; Sawaya, S.; Akita, S.; Nakayama, Y. Carbon Nanotube Oscillators Toward Zeptogram Detection. *Appl. Phys. Lett.* **2005**, *86*, No. 133111.
7. Truitt, P. A.; Hertzberg, J. B.; Huang, C. C.; Ekinci, K. L.; Schwab, K. C. Efficient and Sensitive Capacitive Readout of Nanomechanical Resonator Arrays. *Nano Lett.* **2007**, *7*, 120–126.
8. Han, J.; Henry, T.; Kim, K.; Ren, Z.; Yerino, C.; Tang, H. X. Directed Growth of Horizontally Aligned Gallium Nitride Nanowires for Nanoelectromechanical Resonator Arrays. *Nano Lett.* **2007**, *7*, 3315–3319.
9. Cleland, A. N.; Geller, M. R. Superconducting Qubit Storage and Entanglement with Nanomechanical Resonators. *Phys. Rev. Lett.* **2004**, *93*, No. 070501.
10. Chiu, H. Y.; Hung, P.; Postma, H. W. C.; Bockrath, M. Atomic-Scale Mass Sensing Using Carbon Nanotube Resonators. *Nano Lett.* **2008**, *8*, 4342–4346.
11. Huttel, A. K.; Steele, G. A.; Witkamp, B.; Poot, M.; Kouwenhoven, L. P.; van der Zant, H. S. J. Carbon Nanotubes as Ultrahigh Quality Factor Mechanical Resonators. *Nano Lett.* **2009**, *9*, 2547–2552.
12. Ayari, A.; Vincent, P.; Perisanu, S.; Choueib, M.; Gouttenoire, V.; Bechelany, M.; Cornu, D.; Purcell, S. T. Self-Oscillations in Field Emission Nanowire Mechanical Resonators: A Nanometric DC-AC Conversion. *Nano Lett.* **2007**, *7*, 2252–2257.

13. Weldon, J. A.; Aleman, B.; Sussman, A.; Gannett, W.; Zettl, A. K. Sustained Mechanical Self-Oscillations in Carbon Nanotubes. *Nano Lett.* **2010**, *10*, 1728–1733.
14. Volodin, A.; Buntinx, D.; Ahlskog, M.; Fonseca, A.; Nagy, J. B.; Van Haesendonck, C. Coiled Carbon Nanotubes as Self-Sensing Mechanical Resonators. *Nano Lett.* **2004**, *4*, 1775–1779.
15. Ilic, B.; Krylov, S.; Kondratovich, M.; Craighead, H. G. Optically Actuated Nanoelectromechanical Oscillators. *IEEE J. Sel. Top. Quantum Electron.* **2007**, *13*, 392–399.
16. Then, D.; Vidic, A.; Ziegler, C. A Highly Sensitive Self-Oscillating Cantilever Array for the Quantitative and Qualitative Analysis of Organic Vapor Mixtures. *Sens. Actuators, B* **2006**, *117*, 1–9.
17. Ono, T.; Esashi, M. Magnetic Force and Optical Force Sensing with Ultrathin Silicon Resonator. *Rev. Sci. Instrum.* **2003**, *74*, 5141–5146.
18. Moreland, J. Micromechanical Instruments for Ferromagnetic Measurements. *J. Phys. D: Appl. Phys.* **2003**, *36*, R39–R51.
19. Sidles, J. A.; Garbini, J. L.; Bruland, K. J.; Rugar, D.; Zuger, O.; Hoen, S.; Yannoni, C. S. Magnetic-Resonance Force Microscopy. *Rev. Mod. Phys.* **1995**, *67*, 249–265.
20. Suter, A. The Magnetic Resonance Force Microscope. *Prog. Nucl. Magn. Reson. Spectrosc.* **2004**, *45*, 239–274.
21. Volodin, A.; Van Haesendonck, C.; Tarkiainen, R.; Ahlskog, M.; Fonseca, A.; Nagy, J. B. AFM Detection of the Mechanical Resonances of Coiled Carbon Nanotubes. *Appl. Phys. A: Mater. Sci. Process.* **2001**, *72*, S75–S78.
22. Parker, T. C.; Tang, F.; Wang, G. C.; Lu, T. M. Non-Contact Atomic Force Microscopy Characterization of Micro-Cantilevers and Piezo Electric Transducers with Frequencies up to the Tens of MHz. *Sens. Actuators, A* **2008**, *148*, 306–310.
23. Garcia-Sanchez, D.; Paulo, A. S.; Esplandiu, M. J.; Perez-Murano, F.; Forro, L.; Aguasca, A.; Bachtold, A. Mechanical Detection of Carbon Nanotube Resonator Vibrations. *Phys. Rev. Lett.* **2007**, *99*, 085501–4.
24. Santini, C. A.; Vereecken, P. M.; Volodin, A.; De Gendt, S.; Groeseneken, G.; Van Haesendonck, C. A Study of Joule Heating-Induced Breakdown of Carbon Nanotube Interconnects. *Nanotechnology* **2011**, *22*, 395202–9.
25. Santini, C. A.; Cott, D. J.; Romo-Negreira, A.; Riva-Sanseverino, S.; De Gendt, S.; Vereecken, P. M. Growth and Electrical Characterisation of Horizontally Aligned CNTs. *ECS Trans.* **2009**, *18*, 845–850.
26. Santini, C. A.; Cott, D. J.; Romo-Negreira, A.; Capraro, B. D.; Sanseverino, S. R.; De Gendt, S.; Groeseneken, G.; Vereecken, P. M. Growth and Characterization of Horizontally Suspended CNTs Across TiN Electrode Gaps. *Nanotechnology* **2010**, *21*, 245604–9.
27. Santini, C. A.; Volodin, A.; Van Haesendonck, C.; De Gendt, S.; Groeseneken, G.; Vereecken, P. M. Carbon Nanotube - Carbon Nanotube Contacts as an Alternative Towards Low Resistance Horizontal Interconnects. *Carbon* **2011**, *49*, 4004–4012.
28. Rugar, D.; Yannoni, C. S.; Sidles, J. A. Mechanical Detection of Magnetic-Resonance. *Nature* **1992**, *360*, 563–566.
29. Kuehn, S.; Hickman, S. A.; Marohn, J. A. Advances in Mechanical Detection of Magnetic Resonance. *J. Chem. Phys.* **2008**, *128*, No. 052208.
30. De Biasi, E.; Leon-Vanegas, A.; Nunes, W. C.; Sharma, S. K.; Haddad, P.; Rocha, T. C. R.; Santos Duque, J. G.; Zanchet, D.; Knobel, M. Complex Magnetic Internal Order in Structurally Disordered Ni Nanoparticles. *Eur. Phys. J.* **2008**, *B 66*, 503–508.
31. Sparks, M. *Ferromagnetic Relaxation Theory*; McGraw-Hill: New York, 1964.
32. Sarid, D. In *Scanning Force Microscopy with Applications to Electric, Magnetic and Atomic Forces*; Oxford University Press: New York, 1994; pp 12−17.
33. Gaillard, J.; Skove, M.; Rao, A. M. Mechanical Properties of Chemical Vapor Deposition-Grown Multiwalled Carbon Nanotubes. *Appl. Phys. Lett.* **2005**, *86*, No. 233109.
34. Ekinci, K. L.; Yang, Y. T.; Roukes, M. L. Ultimate Limits to Inertial Mass Sensing Based upon Nanoelectromechanical Systems. *J. Appl. Phys.* **2004**, *95*, 2682–2689.
35. Dijon, J.; Szkutnik, P. D.; Fournier, A.; Goislard de Monsabert, T.; Okuno, H.; Quesnel, E.; Muffato, V.; De Vito, E.; Bendiab, N.; Bogner, A.; Bernier, N. How To Switch From a Tip to Base Growth Mechanism in Carbon Nanotube Growth by Catalytic Chemical Vapour Deposition. *Carbon* **2010**, *48*, 3953–3963.